Optical resonances in periodic surface arrays of metallic patches

W. L. Schaich, G. Schider, J. R. Krenn, A. Leitner, F. R. Aussenegg, I. Puscasu, B. Monacelli, and G. Boreman

The transmission of light along the surface normal through an air–quartz-glass interface covered with a periodic array of thin, rectangular gold patches has been studied over the visible to infrared range. The various structures that are observed can be qualitatively understood as arising from standing-wave resonances set by the size and surroundings of the metal patches. A method-of-moments calculational scheme provides simulations in good quantitative agreement with the data. It is shown how the standing-wave picture provides a useful conceptual framework to understand and exploit such systems.

OCIS codes: 260.3060, 300.6490, 240.6680, 260.1960.

1. Introduction

In this paper the interaction of light with a layer of conducting particles is studied. The specific, simple system under consideration is illustrated in Fig. 1 where the particles are thin, rectangular patches of metal, fixed in a periodic rectangular array on a transparent, flat substrate. Our interest is in understanding the possible optical resonances that can occur when light (polarized along the long patch dimension, for example) is incident along the surface normal. Over narrow ranges of (vacuum) wavelength λ, there will be enhanced reflection and absorption, with a corresponding reduction of transmission.

The interpretation of the physics involved in such resonances depends on the relative size of λ and the long dimension w_y. We focus here on the spectral range where λ is comparable to w_y. As a first approximation, consider a single patch in isolation. It can be viewed as an antenna that supports various standing waves. The simplest estimate for the location of these is $j(\lambda/2) = w_y$, where j is an integer. The strongest resonance is the first, $j = 1$, or dipole resonance. Its associated current profile has nodes at each end of a patch and a single antinode in the center. This sort of picture is most reasonable in the infrared and longer-wavelength range, where metals behave as (near-) perfect conductors. Many systems have been studied in this limit, usually under the name of frequency-selective surfaces.[1–3] More recent research has been moving toward shorter wavelengths.[4,5]

Of course the resonance locations also depend on the other parameters of the model such as the remaining dimensions of the patch, width w_z, and thickness h; the periods of the surface array d_y and d_z; the optical index of the glass substrate $n_g = [\epsilon_g/\epsilon_0]^{1/2}$; and the dielectric response of the metal. Several studies have compared experiment and theory with regard to these dependencies,[6–11] but they have concentrated mostly on the dipole resonance. Here we examine a series of resonances to learn how well they can be understood in the standing-wave picture. As the mode index j is increased (or w_y is decreased), the resonance wavelength will decrease and the material dependence of the metal's response should become more important. Indeed, with $w_y \sim 1$ μm, one readily encounters resonance frequencies comparable to the bulk plasma frequency as j increases.

W. L. Schaich (schaich@indiana.edu) is with the Department of Physics, Indiana University, Bloomington, Indiana 47405. G. Schider, J. R. Krenn, A. Leitner, and F. R. Aussenegg are with the Institute for Experimental Physics, Karl-Franzens University and the Erwin Schrödinger Institute for Nanoscale Research, Universitätsplatz, Graz A-8010, Austria. When this research was performed, I. Puscasu, B. Monacelli, and G. Boreman were with the School of Optics, Center for Research and Education in Optics and Lasers, University of Central Florida, 4000 Central Florida Boulevard, Orlando, Florida 32816. I. Puscasu is now with Ion-Optics, 411 Waverly Oaks Road, Suite 144, Waltham, Massachusetts 02452.

Received 16 October 2002; revised manuscript received 16 April 2003.

0003-6935/03/285714-08$15.00/0

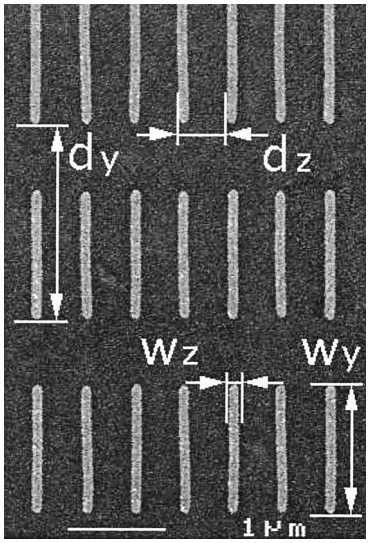

Fig. 1. Scanning electron micrograph of a patch array.

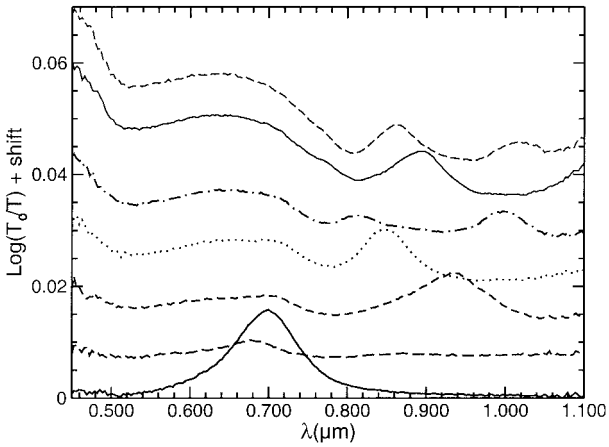

Fig. 2. Extinction versus vacuum wavelength for different values of w_y. Results for successive patterns are shifted by 0.005, and each pattern was fabricated and measured twice at different places on the substrate. Moving from the bottom to the top curves, the values of w_y are 0.091, 0.32, 0.58, 0.85, 1.10, 1.34, and 1.62 μm. The value of $w_z = 0.091$ μm.

To study a series of resonances one needs to measure over a broad spectral range. This is accomplished by use of different instruments for the visible and infrared ranges. In Section 2 we describe these measurements along with our sample preparation methods. The theoretical model for calculations of the system's optical response is outlined in Section 3 where we generalize an approach developed earlier to simulate spectra near dipole resonances in the infrared.[10] The theory predicts a whole transmission spectrum, T versus λ, and hence can be directly compared with experimental data. Finally, in Section 4 we summarize what has been learned by such comparisons and note several implied features that deserve further study. We conclude that a standing-wave picture does provide useful insights, and our detailed simulations do agree well with the measurements.

2. Sample Fabrication and Measurement

The basic sample configuration is shown in Fig. 1. The metal patches are made of gold, deposited by electron-beam lithography in Graz, Austria, on a quartz-glass substrate 1 mm thick that was doped with indium tin oxide over a depth of 3 nm. Details on this technique can be found in Ref. 12. For the measurements described here only the long dimension of the metal patches was varied. The other parameters were fixed at the nominal values of $w_z = 91$ nm, $h = 17$ nm, $d_y = 2.11$ μm, and $d_z = 0.54$ μm. These geometric parameters have an uncertainty of several percent.

Because the total extent for a particular pattern is a 150-μm square, special care is necessary to measure the optical response. In the visible range, extinction spectra of linearly polarized light are measured with a Carl Zeiss MMS1 spectrometer coupled to a conventional optical microscope equipped with a low-numerical-aperture (0.075) objective. Hence the greatest deviation from normal incidence of any light that can be collected is 4.3°.

Results for a set of patterns of varying w_y are shown in Fig. 2. The polarization of the incident light is along the y direction and the T_0 that appears in the extinction definition is the transmission through a region of the substrate where there are no metal patches. Working with T_0/T provides a convenient normalization that suppresses variations independent of the patch pattern, which are not of interest here. The resonances of interest are associated with the extinction peaks. These are evident only for $\lambda \geq 700$ nm; in earlier studies with Ag patches, peaks were observed down to 500 nm.[13]

Measurements in the infrared of the same samples were made with the Perkin-Elmer Fourier-Transform Spectrum 2100 at Agere Systems in Orlando, Florida. The incident light was unpolarized, and because it was focused with an $F/3.2$ lens into a 100-μm-diameter spot through the center of a pattern on the surface, its path could deviate by up to 9° away from the surface normal. Again we work with only the relative transmission T/T_0. Plots of T/T_0 versus λ for different choices of w_y are given in Section 3 where they are compared with the simulations.

3. Theoretical Model

The calculational scheme we use is based on a specialization of the general formalism that has been developed for frequency-selective surfaces.[1] The main ideas have been described earlier,[10,11] so we discuss only modifications that were made for the present study. We concentrate on the transmission coefficient for a beam to cross the patterned vacuum–glass interface without deflection. Multiple reflections within the glass are ignored. It was demonstrated in Ref. 11 that such processes are of little quantitative significance. We also ignore any

possible optical effects of the indium tin oxide doping layer.

The metal patches are treated as negligibly thin but possessing a complex-valued sheet resistance $R = 1/\Sigma$. The conductance Σ is calculated from

$$Z_0\Sigma = -2\pi i(\epsilon/\epsilon_0 - 1)\frac{h}{\lambda}, \tag{1}$$

where ϵ is the dielectric function of the metal and $Z_0 = [\mu_0/\epsilon_0]^{1/2} \approx 377\ \Omega$ is the impedance of free space. If the metal's response at frequency ω were described simply by a conductivity σ, then $\epsilon = \epsilon_0 + i\sigma/\omega$ and Σ would be σh. For gold we start with the Drude form

$$\epsilon = \epsilon_d - \epsilon_0\omega_p{}^2/[\omega(\omega + i/\tau)], \tag{2}$$

where $\epsilon_d/\epsilon_0 = 8$ characterizes the polarization of the d electrons and the free-electron response is described by the plasma frequency $\hbar\omega_p = 8$ eV and a scattering rate $1/\tau$. Such a functional form provides a reasonable fit to the bulk optical data of gold,[14–16] if we use $1/\omega_p\tau = 0.008$, and gives us the freedom to tweak ϵ with physically understandable parameters. In particular we show below that $1/\tau$ for the thin metal patches must be significantly increased if our theory is to reproduce the transmission data for the patterned surfaces.

In earlier calculations[10,11] with the incident electric polarization along the y direction, we constrained the induced current in the metal patches to be only along $\hat{y}$ and to be independent of z. Here we allow for a more general (but still two-dimensional) current pattern. Again, with the incident electric field along $\hat{y}$, we write for the current density within each patch

$$J_y(y, z) = \sum_{j,k} d_{j,k}^{(y)} \cos\left(j\frac{\pi}{2}\tilde{y}\right)\cos\left(k\frac{\pi}{2}\tilde{z}\right), \tag{3}$$

$$J_z(y, z) = \sum_{j,k} d_{j,k}^{(z)} \sin\left(j\frac{\pi}{2}\tilde{y}\right)\sin\left(k\frac{\pi}{2}\tilde{z}\right), \tag{4}$$

where $\tilde{y} = 2y/w_y$ and $\tilde{z} = 2z/w_z$ with the origin for y and z in the center of a patch. The j's and k's are nonnegative integers with the j's odd and the k's even. The value $k = 0$ is to be included in Eq. (3), but not in Eq. (4). With these choices, J_y vanishes at the extreme values $|\tilde{y}| = 1$, and J_z vanishes at the extreme values $|\tilde{z}| = 1$. On the other hand the current flow parallel to an edge (J_y along $|\tilde{z}| = 1$ or J_z along $|\tilde{y}| = 1$) is nonzero and can be enhanced.[17] The symmetries of the currents under $y \to -y$ or $z \to -z$ are correct if the light is incident along the surface normal; otherwise basis functions of different parity need to be included. The expansion coefficients $d_{j,k}^{(\alpha)}$ in Eqs. (3) and (4) are determined by the Galerkin version of the method of moments.[18] With them the currents are known, and one can readily find the transmission coefficient of the beam moving along the surface normal into the glass substrate. The same relative transmission is obtained if the beam is incident from the glass, which in fact is the direction used in the measurements.

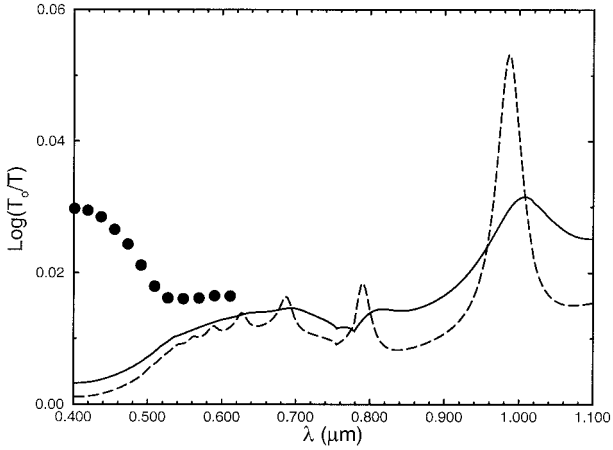

Fig. 3. Calculated extinction versus wavelength for $w_y = 1.10$ μm. The solid (dashed) curve is calculated with a scattering rate $1/\omega_p\tau = 0.024$ (0.008) and patch thickness $h = 16$ nm (17 nm). See text for other parameter values. The circles are from a calculation that uses a tabulated (rather than Drude) dielectric function plus $h = 16$ nm.

Typical results are shown in Fig. 3 for incident light polarized along $\hat{y}$. We use here (and below) a spline interpolation through tabulated values[16] of ϵ_g/ϵ_0 for the quartz-glass substrate. The long dimension of the patch is $w_y = 1.10$ μm, and we plot the extinction as in Fig. 2 (but without a shift of 0.02). For the initial calculation we used the stated values of all the parameters defined above. However, the resulting peaks are too strong and sharp. The form of the peaks is better reproduced if we increase the Drude scattering rate by approximately a factor of 3. To better match the peak locations, we reduced the patch thickness from its nominal value $h = 17$ nm to $h = 16$ nm. The direction of these two modifications is not unreasonable. One expects there to be extra (surface) scattering in the thin patches, and their vertical profile is somewhat rounded rather than rectangular. However, the specific values of $1/\tau$ and h that we use were chosen simply to produce a better match with the data of Fig. 2. Because the Drude representation of ϵ in Eq. (2) becomes increasingly poor as one crosses the interband threshold, we stop our calculation at $\lambda = 500$ nm. However, there is a clear upturn in extinction for shorter wavelengths in Fig. 2, so we also calculated what our model would predict if the optical data of Johnson and Christy[14] are used for ϵ. It appears that the onset of additional absorption in bulk gold below 500 nm does account for the observed enhanced extinction.

Next we hold fixed all parameters except w_y and calculate for Fig. 4 the analog of the measured Fig. 2. There is reasonable agreement between the two plots, particularly for the location and shape of the several peaks evident at longer wavelengths. For each of the calculated curves, we used $1/\omega_p\tau = 0.024$ and $h = 16$ nm plus the nominal values of the other parameters. The slight disagreement between the-

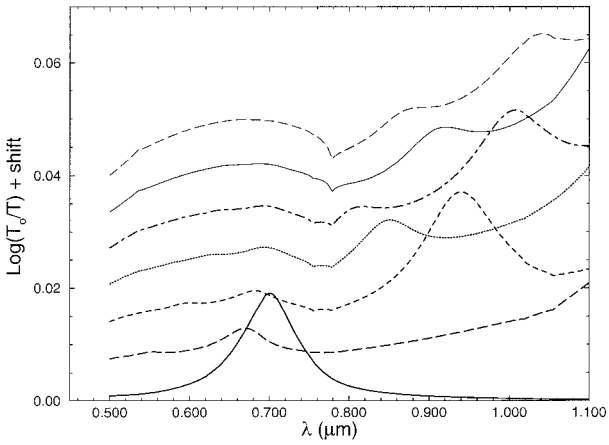

Fig. 4. Calculated extinction versus wavelength for various w_y. Results for successive patterns are shifted by 0.005. The labeling scheme is the same as in Fig. 2.

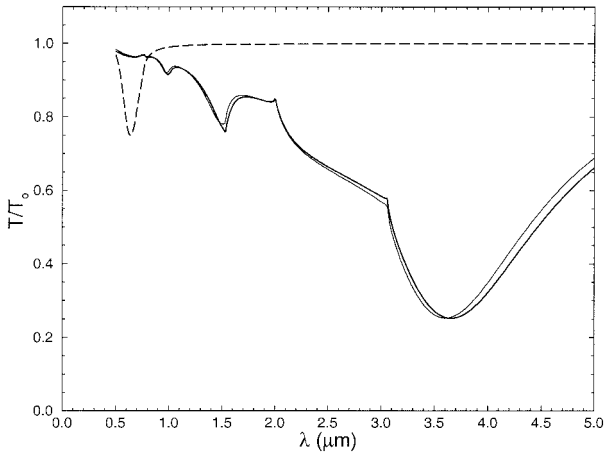

Fig. 5. Calculated relative transmission versus wavelength for $w_y = 1.10$ μm. For the solid (dashed) curve the incident polarization is along the y (z) direction. For the thin solid curve the current is allowed to flow only along $\hat{y}$ and is independent of z within a patch.

ory and experiment for the peaks seems to be an oscillatory function of w_y. The peaks are stronger and sharper in the calculations compared with the data for $w_y = 1.10$ and 0.58 μm but are weaker and broader for $w_y = 1.34$ and 0.85 μm. This may be related to the fact that the calculated peaks are riding on a rising background at longer wavelengths whereas in the data the background level is roughly constant. We do not have a reason for this difference. The discrepancies at the shortest wavelengths have already been discussed in reference to Fig. 3. They arise from the inadequacy of the Drude parameterization in this λ limit.

Finally we comment on the kink in the extinction curves that appears near λ = 776 nm for all but the shorter values of w_y. Our interpretation of this structure is that it is a grating effect that is due to the periodic array of patches.[19] Also called a Rayleigh–Wood (or more simply, threshold) anomaly,[20] it arises from the following physics. We are determining the transmission of the beam that is undeflected (undiffracted) by the surface. However, as the wavelength is decreased, one sweeps through thresholds at which other (diffracted) beams become able to propagate away from the surface. As each threshold is crossed the undeflected beam intensity often exhibits a kink-like structure. The location of these kinks is easy to predict,[10] but the precise shape and strength of any such structure requires detailed calculation. The kink at λ = 776 nm arises from a first-order diffraction in the z direction entering the glass substrate. Its location is given by $n_g d_z = (1.45)(535\text{ nm}) = 776$ nm. Several other such anomalies are occasionally evident in the calculations. For example, the structure at λ = 1.055 μm arises from a second-order diffraction in the y direction scattered into vacuum because $d_y/2 = 1.055$ μm. Still more structures appear in the infrared, to which we now turn.

We continue to use the same geometric and material parameters. The only difference is that we extend the wavelength range where resonances are sought. To give an overview, consider Fig. 5 that shows the relative transmission for a particular $w_y = 1.10$ μm and different polarizations. For orientation, the dip just above λ = 1 μm corresponds to the extinction peak in Fig. 3. As the wavelength is increased there are two additional resonances at λ = 1.52 and 3.66 μm and more threshold anomalies at λ = 1.54, 2.11, and 3.04 μm. The near overlap of a resonance and a threshold anomaly near 1.54 μm is a coincidence. These further resonances are much stronger and broader than the ones in the visible. Note that use of a more limited basis set to expand the induced currents is of little importance. The second curve for y polarization is calculated with the more restricted expansion of Ref. 10.

The response to light polarized along $\hat{z}$ is negligible through most of the infrared. A standing wave is still possible but its location is set by w_z, which is much smaller than most w_y values and hence first appears in the visible at λ = 629 nm. The structure of Fig. 5 shows that measurements with unpolarized light in the infrared can be directly interpreted in terms of resonances with the driving field along $\hat{y}$. We use

$$T^{(\mathrm{un})}/T_0^{(\mathrm{un})} = \frac{1}{2}\left[T^{(y)}/T_0^{(y)} + T^{(z)}/T_0^{(z)}\right] \approx \frac{1}{2}\left[T^{(y)}/T_0^{(y)} + 1\right], \quad (5)$$

where the y or z superscripts describe directions of the incident polarization and un denotes unpolarized.

Now compare the experiment and theory in the infrared. Results for different patterns are shown in the different panels of Fig. 6. We stress that the parameter choices in the calculations are the same as for Fig. 4. Overall the agreement continues to be good, in particular for the location and depth of the main resonance. The theory also reproduces some of the smaller structures, e.g., in (a), (b), (c), and (d) at

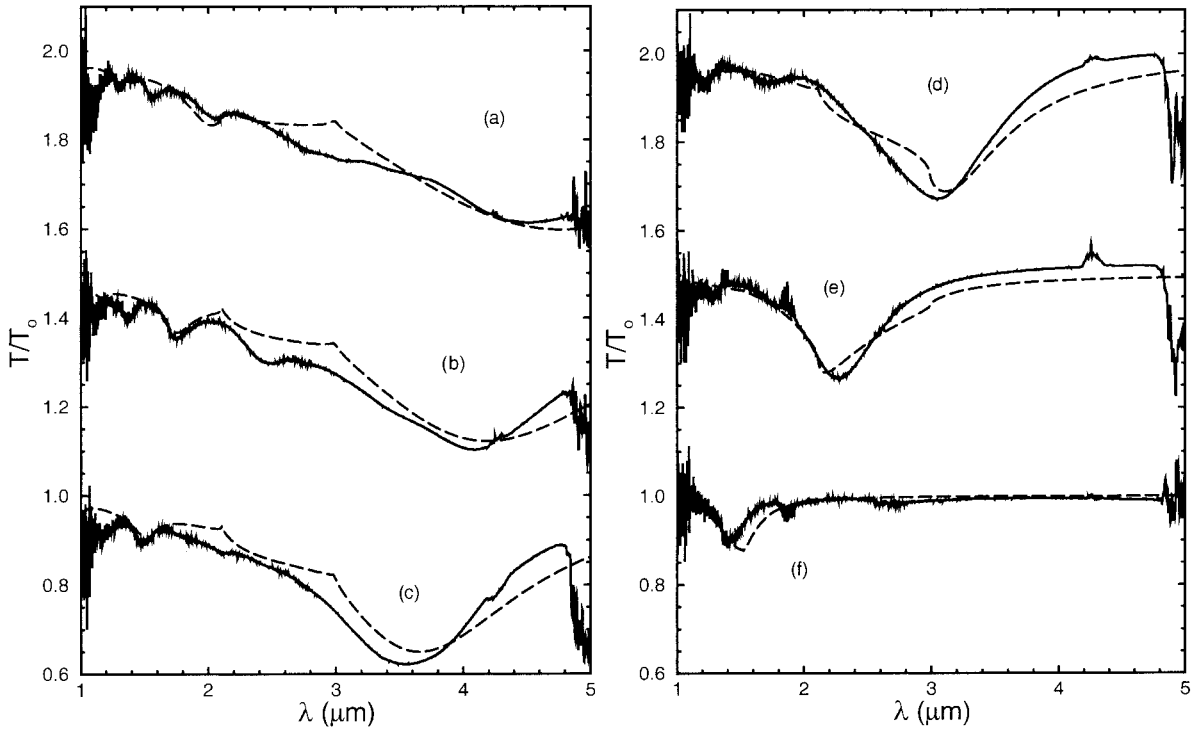

Fig. 6. Relative transmission versus wavelength for unpolarized incident light. The dashed curve is from the model calculation based on Eq. (5). The values of w_y in micrometers are (a) 1.62, (b) 1.34, (c) 1.10, (d) 0.85, (e) 0.58, and (f) 0.32. Results for different w_y are shifted by 0.5.

λ = 1.32, 1.74, 1.52, and 1.20 μm, respectively. As for disagreements, we note three general features. First, the theoretical transmission for wavelengths longer than the main resonance location is less than the measured transmission. Second, most of the kinks that are due to threshold anomalies in the simulations do not appear in the measurements. Third, there are additional local minima in the data around 1.55, 1.35, 1.1, and 1.7 μm in (a)–(d), respectively, that are missing in the calculations.

The resolution of the last two kinds of puzzle might lie with the spread of incident angles in the measurements. As noted in Section 2, the infrared arrangement allows light at up to 9° away from normal incidence to be collected. For a rough estimate of the consequences of this spread on the simulations, we performed some calculations with an incident beam away from the normal, but confined to the x–y plane. Results are shown in Fig. 7. Note first that the threshold anomalies split and shift as the angle of incidence θ is varied. This occurs because the criterion for their appearance in our special geometry is

$$(\epsilon/\epsilon_0)^{1/2}\frac{2\pi}{\lambda} = \left|\underset{\sim}{G} + \hat{y}\,\frac{2\pi}{\lambda}\sin\theta\right|, \tag{6}$$

where λ is the vacuum wavelength, ϵ is either ϵ_0 or ϵ_g, and

$$\underset{\sim}{G} = 2\pi\left(\frac{n_y}{d_y}\hat{y} + \frac{n_z}{d_z}\hat{z}\right) \tag{7}$$

is a two-dimensional reciprocal lattice vector of the patch array with n_y and n_z integers. The net influence of threshold anomalies will be reduced by an average over incident angles. Note too that the minimum in T/T_0 near 2 μm shifts to longer wavelengths (and better agreement with the data) as θ increases. This happens because of an accidental overlap of the $\theta = 0$ threshold anomaly at 2.11 μm with an isolated patch resonance. As θ increases, the overlap and consequent distortion are reduced.

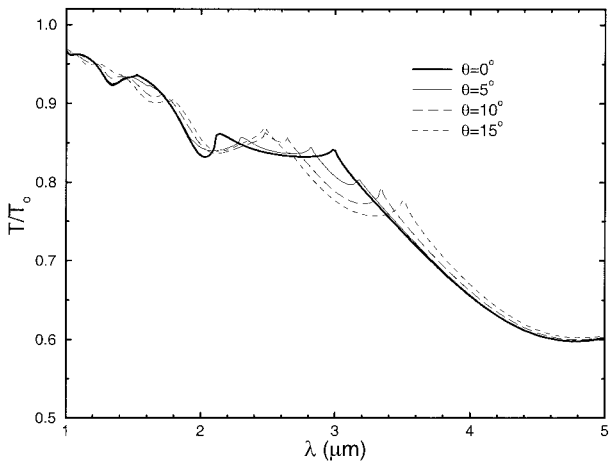

Fig. 7. Calculated transmission versus wavelength for w_y = 1.62 μm. The light is incident in the x–y plane at an angle θ with respect to the surface normal. We use Eq. (5) for the unpolarized light. The $\theta = 0$ result is the same as the theory curve in Fig. 6(a).

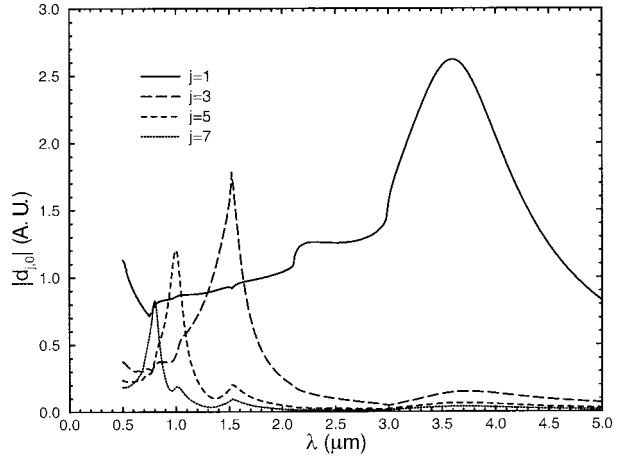

Fig. 8. Expansion coefficients versus wavelength for $w_y = 1.10$ μm. The location of structures correlates well with the minima and threshold anomalies in the T/T_0 of Fig. 5.

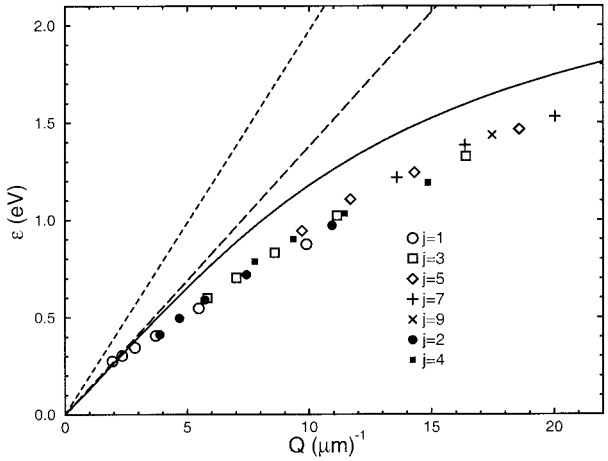

Fig. 9. Possible surface dispersion of resonance locations $\epsilon = \hbar\omega$ versus wave vector Q. The points are extracted from the results of Figs. 2 and 6 by Eq. (9). Some even j modes, excited off normal incidence in the infrared, are included. The long- (short-) dashed curves are the light lines for glass (vacuum). At frequencies above them light can propagate away from the surface. The solid curve is the (lowest) retarded surface plasmon for a homogeneous Au layer of thickness $h = 16$ nm between vacuum and glass.

A further development with increasing θ is the appearance of additional resonance minima in between those present at $\theta = 0$. In Fig. 7, these extra minima occur at 1.17, 1.67, and perhaps 3.3 μm. They arise from the broken symmetry for $\theta \neq 0$ that leads to additional basis terms in the expansion of J_y in Eq. (3) of the form $d_{j,k}^{(y)} \sin j(\pi/2)\tilde{y} \cos k(\pi/2)\tilde{z}$ where both j and k are even integers. Compared with the experiment, the new modes are appearing in approximately the right places, but it is not fair to draw a definite conclusion because the calculations have not averaged over all possible incident directions and it is difficult to differentiate the new minima from threshold anomalies and measurement noise.

4. Discussion

In our comparisons so far of experiment and theory we have made little reference to the standing-wave picture described in Section 1. The reason for this is because the utility of that picture lies primarily in the conceptual overview it provides rather than in its specific numerical estimates. More sophisticated models, such as the one described in Section 3, are needed to produce reliable quantitative results. Nevertheless it is helpful to have the picture in mind as one attempts to understand and predict possible behaviors.

The standing-wave index j corresponds to the j index appearing in Eq. (3). With incident light polarized along $\hat{y}$, the $d_{j,k}^{(y)}$ on resonance will be enhanced for a particular j. This is illustrated in Fig. 8 that plots the magnitude of the complex amplitudes $|d_{j,k=0}^{(y)}|$ versus λ for several (odd) values of j. These were chosen because the transmission changes are controlled by the spatial average of the induced current. From Eq. (3) this involves

$$\int_{-1}^{1} d\tilde{y} \int_{-1}^{1} d\tilde{z} J_y(y, z) = \frac{8}{\pi} \sum_j d_{j,0}^{(y)} (-1)^{\frac{j-1}{2}}/j, \quad (8)$$

where the sum is over odd values of j. Compared with Fig. 5, we can see that, at different resonant minima in T/T_0, different values of j dominate. Thus the sequence of resonances can be labeled with successive odd integers. It would be interesting to look for the distinct near-field patterns associated with each resonance.

To understand the actual mode locations, we need to generalize the simple formula of the introduction. Of course one cannot use just the vacuum, glass, or metal wavelength to form a standing wave, so we write instead

$$j\left(\frac{\pi}{w_y}\right) = \frac{2\pi}{\lambda_{\text{eff}}} = Q(\omega) \quad (9)$$

and use our results to determine the dispersion of the effective wave established near the patch. Thus we are not trying (yet) to predict the effective wavelength, but instead we are checking whether there is a common dispersion curve $\omega(Q)$ for different j and w_y that underlies all the observed resonances. Results from the measurements of Figs. 2 and 6 are collected in Fig. 9, which demonstrates that Eq. (9) does allow the resonance locations of various orders to be scaled onto a single curve.

The appearance of Fig. 9 is appealing and raises the further question as to whether the effective dispersion relation can be derived. As a first guess consider the nonretarded surface plasmon produced by a thin homogeneous layer of free electrons located at the interface between two dielectrics. For wave vector Q within the plane,[21]

$$\omega^2 = {\omega_p}^2 Q h \left(\frac{\epsilon_0}{\epsilon_g + \epsilon_0}\right), \quad (10)$$

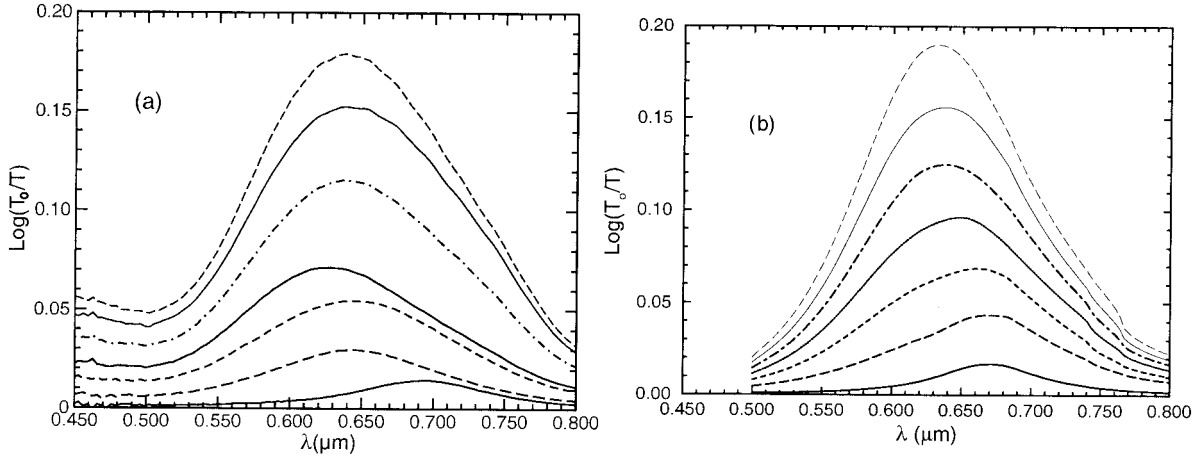

Fig. 10. Extinction versus wavelength for different values of w_y with incident polarization along $\hat{z}$. The theoretical curves in (b) are calculated with the same parameters used for Figs. 4 and 6.

where ω_p is the plasma frequency of the free electrons in bulk, h is the thickness of the metal layer, and we assumed that the two bounding dielectrics are vacuum and glass. Equation (10) is qualitatively correct but quantitatively unreliable. We need to allow at least for the dielectric response of gold [by using the ϵ of Eq. (2)] and to include retardation. An analytic result is then not possible but a numerical dispersion can be obtained by the scheme of Ref. 22. For wave vector Q within the plane, fields away from the interface vary as $\exp[i(Qy - \omega t)]\exp(-\bar{Q}|x|)$ where t is time, x is along the surface normal, and

$$\bar{Q} = \left(Q^2 - \frac{\omega^2}{c^2} \frac{\epsilon}{\epsilon_0} \right)^{1/2}, \tag{11}$$

with $\epsilon = \epsilon_g(\epsilon_0)$ in glass (vacuum). If one perturbs the surface with such an incident wave holding Q fixed and varying ω, then the reflected wave will show a resonant peak as ω crosses the surface mode.

Results from such a procedure were also plotted in Fig. 9 with a constant $n_g = 1.43$. For larger Q the calculated curve is significantly above the data points. Use of Eq. (10) makes the discrepancy worse. In the opposite limit, theory and experiment seem to merge, or perhaps cross, as $Q \to 0$. Because we are looking in the calculation for a mode bound to the surface, the theoretical curve cannot cross the light line of glass that is defined by the vanishing of $\bar{Q}$ in Eq. (11). However, the measured points are not so constrained and may indeed come from resonances in the continuum. The problem is that the patterned surface couples different wave vectors together so estimates of $\omega(Q)$ based on models of a homogeneous metal layer supporting a single Q cannot be expected to succeed.[23] Another way of appreciating the problem is to recall that it has been shown[10,19] that the shapes and locations of resonances depend on the lattice constants of the patch array. This can be viewed as arising from threshold anomalies or more simply from the interactions of different patches by their electrodynamic fields. The consequent distortions are larger for modes with smaller j because the standing-wave pattern influences the range of the near fields. Given all these points of view it is clear that one must expect some imprecision in the standing-wave picture.

There are other ways in which the utility and the limitations of the standing-wave picture appear together. Consider, for example, the response to light polarized along the short dimension of the patches. A first estimate would be to use Eq. (9) with $w_y \to w_z$, so one would expect for our samples that the resonances would be independent of w_y and off the scale of Fig. 9 because the minimum Q would be $\pi/(0.091\ \mu\text{m}) = 34.5\ (\mu\text{m})^{-1}$. In Fig. 10 we compare experiment and theory for the extinction of $\hat{z}$ incident polarization. We identify the single peak in all cases as arising from the $j = 1$ dipole excitation. The location of this peak is a weak monotonic function of w_y in the simulations but appears slightly nonmonotonic in the data. The relative heights of the peaks compare well, decreasing with the amount of metal on the surface. There is no evidence of higher-order peaks, probably because these would be at or beyond the threshold for d-band excitations.

The extinction data for different incident polarizations could be used to make an interesting check of the consistency of the standing-wave picture. Imagine producing the same Q in two different ways:

$$j_y \frac{\pi}{w_y} = Q = j_z \frac{\pi}{w_z}. \tag{12}$$

Then one should expect that simply by switching between two orthogonal incident polarizations it would be possible to excite one or the other of two degenerate modes. In the standing-wave picture this novel situation arises whenever w_y/w_z is the ratio of small odd integers. We almost have such a case in Figs. 2 and 10 when the extinction peak for $w_y = 0.32\ \mu\text{m}$ and $j_y = 3$ nearly overlaps that for $j_z = 1$. A more focused study of this effect is postponed to a future study. We expect with the quantitative imprecision

of the standing-wave picture that one will need a series of samples with ω_y/ω_z close to the required ratio from Eq. (12) to find a sample where the resonances for orthogonal polarizations exactly coincide.

To summarize, we have measured optical transmission over a wide spectral range through surfaces covered with a periodic array of metal patches. Detailed simulations can successfully reproduce the principal features of the data. In addition we have shown how a standing-wave picture of the resonances provides a helpful overview of the physics, aiding the interpretation and suggesting new ways to examine and exploit these systems.

Some of the calculations were performed on the Cray Research Incorporated T90 system at the National Partnership for Advanced Computational Infrastructure, San Diego, Calif. Partial support for this research was provided by NASA under grant NAG5-10308 (I. Puscasu, B. Monacelli, and G. Boreman) and by the Austrian Ministry for Technology and the Austrian Science Foundation (G. Schider, J. Krenn, A. Leitner, and F. R. Aussenegg).

References

1. R. Mittra, C. H. Chan, and T. Cwik, "Techniques for analyzing frequency selective surfaces—a review," Proc. IEEE **76,** 1593–1615 (1988).
2. J. C. Vardaxoglou, *Frequency Selective Surfaces: Analysis and Design* (Research Studies, Taunton, UK, 1997).
3. T. K. Wu, *Frequency Selective Surface and Grid Array* (Wiley, New York, 1995).
4. V. Kettunen, M. Kuittnen, J. Tarunen, and P. Vahimaa, "Spectral filtering with finitely conducting inductive grids," J. Opt. Soc. Am. A **15,** 2783–2785 (1998).
5. K. D. Möller, O. Sternberg, H. Grebel, and P. Lahanne, "Thick inductive cross shaped metal meshes," J. Appl. Phys. **91,** 9461–9465 (2002).
6. S. T. Chase and R. D. Joseph, "Resonant array bandpass filters for the far infrared," Appl. Opt. **22,** 1775–1779 (1983).
7. T. Schimert and M. E. Koch, "Analysis of scattering from frequency-selective surfaces in the infrared," J. Opt. Soc. Am. A **7,** 1545–1553 (1990).
8. T. R. Schimert, A. J. Brouns, C. H. Chan, and R. Mittra, "Investigation of millimeter-wave scattering from frequency selective surface," IEEE Trans. Microwave Theory Tech. **39,** 315–322 (1991).
9. I. Puscasu, D. Spencer, and G. Boreman, "Refractive-index and element-spacing effects on the spectral behavior of infrared frequency-selective surfaces," Appl. Opt. **39,** 1570–1574 (2000).
10. I. Puscasu, W. L. Schaich, and G. Boreman, "Modeling parameters for the spectral behavior of infrared frequency-selective surfaces," Appl. Opt. **40,** 118–124 (2001).
11. I. Puscasu, W. L. Schaich, and G. Boreman, "Resonant enhancement of emission and absorption using frequency selective surfaces in the infrared," Infrared Phys. Technol. **43**, 101–107 (2002).
12. W. Gotschy, K. Vonmetz, A. Lectner, and F. R. Aussenegg, "Thin films by regular patterns of metal nanoparticles: tailoring the optical properties by nanodesign," Appl. Phys. B **63**, 381–384 (1996).
13. J. R. Krenn, G. Schider, W. Rechberger, B. Lamprecht, A. Leitner, F. R. Aussenegg, and J. C. Weeber, "Design of multipolar plasmon excitations in silver nanoparticles," Appl. Phys. Lett. **77,** 3379–3381 (2000).
14. P. B. Johnson and R. W. Christy, "Optical constants of the noble metals," Phys. Rev. B **6,** 4370–4379 (1972).
15. M. A. Ordal, L. L. Long, R. J. Bell, S. E. Bell, R. R. Bell, R. W. Alexander, Jr., and C. A. Ward, "Optical properties of the metals Al, Co, Cu, Au, Pb, Ni, Pd, Pt, Ag, Ti, and W in the infrared and far infrared," Appl. Opt. **22,** 1099–1119 (1983).
16. E. D. Palik, *Handbook of Optical Constants of Solids* (Academic, New York, 1985).
17. J. Van Bladel, *Singular Electromagnetic Fields and Sources* (Oxford U. Press, Oxford, UK, 1991).
18. R. F. Harrington, *Field Computation by Moment Methods* (Institute of Electrical and Electronics Engineers, New York, 1992).
19. B. Lamprecht, J. R. Krenn, A. Leitner, and F. R. Aussenegg, "Metal nanoparticle gratings: influence of dipolar particle interaction on the plasmon resonance," Phys. Rev. Lett. **84,** 4721–4724 (2000).
20. R. W. Wood, "Anomalous diffraction gratings," Phys. Rev. **48**, 928–936 (1935).
21. M. G. Cottam and D. R. Tilley, *Introduction to Surface and Superlattice Excitations* (Cambridge U. Press, New York, 1989).
22. M. Cardona, "Fresnel reflection and surface plasmons," Am. J. Phys. **39,** 1277 (1971).
23. Of course one may include the coupling among surface wave vectors and, as shown in Section 3, good agreement is then found for the mode locations.